Disclaimer

This note has not been internally reviewed by the DØ Collaboration. Results or plots contained in this note were only intended for internal documentation by the authors of the note and they are not approved as scientific results by either the authors or the DØ Collaboration. All approved scientific results of the DØ Collaboration have been published as internally reviewed Conference Notes or in peer reviewed journals.

A Study of Electron and Photon Fakes

Steven Glenn
University of California, Davis
5/1/96

1. Introduction

Background estimates to diboson production usually involve counting the jets in inclusive W or Z samples and weighting by the probabilities that a jet is misidentified as a photon or electron to get the estimated number of fake signal events. Previous studies [1-4] with earlier DØ data indicate that the probability for a jet to fake an electron or photon is approximately 10^{-3}, and that the probabilities measured from data roughly agree with the predictions of the ISAJET Monte Carlo [2]. The purpose of this study is to measure the fake rates for the electron/photon identification cuts used in the various run 1B $W\gamma/Z\gamma$ analysis.

At momenta greater than 10 GeV/c, the granularity of the DØ electromagnetic calorimeter is not sufficient to distinguish between isolated $\pi^0/\eta \rightarrow \gamma\gamma$ and single photons on the basis of shower shape* (H-Matrix) or isolation requirements. Therefore, when a jet fragments principally into an isolated π^0 or η, it will be misidentified as an electron or photon. Since the DØ detector has a non-magnetic tracking system, fake electrons will be produced when one or both of the photons convert to an e^+e^- pair via pair production. Similarly, a soft charged hadron from the jet associated with the leading meson (or from the underlying event) near the photon pair will also result in the misidentification of a jet as an electron. (The overlapping hadron must be of low energy for the jet to fake an electron. Otherwise, the prospective fake electron or photon would fail the isolation requirement.)

In this study, fake probabilities are measured from data collected by the single jet filters `jet_20_noL0`, `jet_30`, `jet_50`, `jet_80`, and `jet_max`. To first order, the fake probability is given by the ratio of the jet population to the electron or photon population:

$$P_{j\rightarrow\gamma} \approx N_\gamma/N_j \tag{1}$$

and

$$P_{j\rightarrow e} \approx N_e/N_j \tag{2}$$

where N_γ, N_e, and N_j are the numbers of photons, electrons, and jets, respectively. The jets, electrons, and photons are all counted the same region of phase space. Generally, these

*The H-Matrix χ^2 is dominated by the *transverse* shower shape. Direct photon analyses generally discriminate bewteen single photons and overlapping $\gamma\gamma$ by the *longitudinal* shower shape.

ratios are E_T-dependent, so they must be calculated by bins in E_T. Any angular dependence is assumed to be accounted for by calculating the ratios for the CC and EC separately. It should be noted that the E_T dependences of these ratios are affected by trigger requirements and the presence of real photons in the data due to direct photon production. Sections 3 and 4 describe how these effects are removed.

2. Data Sample and Event Selection

To quantify the frequency at which jets are misidentified as electrons or photons, it is necessary to obtain a data sample which is free of genuine electrons or photons. Since QCD jet cross sections greatly exceed the cross sections for processes which yield authentic electrons or photons, data collected with jet (calorimeter tower) triggers have almost no real[†] e/γ components and are appropriate for this measurement. Therefore, the data used for this study are collected from the `jet_20`, `jet_30`, `jet_50`, `jet_85`, and `jet_max` filters from runs 87804 through 93115. These runs correspond to trigger list versions 10.2 through 10.6. All data were reconstructed with RECO versions 12.15 through 12.20. Jets are reconstructed with a cone size of $\mathcal{R} = 0.5$ and are subject to the following additional requirements:

- $E_T > 10$ GeV
- $|\eta_{\text{Cal.}}| < 1.0$ or $1.5 < |\eta_{\text{Cal.}}| < 2.5$
- $\phi < 1.1$ or $\phi > 1.2$
- Coarse Hadronic (CH) energy $< 40\%$ of total energy
- $E_1/E_2 < 10.0$, where E_1 and E_2 are the two highest energy cells in the cluster.

The first two cuts restrict the jets to the same kinematic phase space as electrons and photons. The ϕ cut eliminates objects caused by Main Ring activity, and the last two cuts remove contributions due to "hot cells" in the calorimeter. Finally, the missing transverse energy is required to be less than 20 GeV to eliminate $W \rightarrow e\nu$ as a possible source of contamination.

[†]Electrons from charm or bottom semileptonic decays are eliminated by the isolation requirement. However, direct photon production is expected to contaminate the sample.

Table 1 summarizes the various tracking criteria for electrons and photons. The kinematic requirements are the same as those used for jets. Each object must also satisfy the following requirements for calorimeter-related variables:

- Electromagnetic Energy Fraction > 0.90
- H-Matrix $\chi^2 < 100$ (200) for CC (EC)
- Fractional Energy Isolation: $I < 0.10$

Object Type	Track Match		Hit Requirement	
	CC	EC	CC	EC
e_t	$s < 5.0$	$s < 10.0$	None	None
e_l	None	None	None	None
$\bar{\gamma}$	None	None	$N_{xy} \geq 20$	$N_{xy} \geq 36$
γ	$s > 5.0$	$s > 10.0$	None	None
γ_t	None	None	$N_{xy} < 20$	$N_{xy} < 36$
PPHO	NoTrk	NoTrk	None	None

Table 1: Summary of track requirements on EM objects. The track match significance is denoted by s, the number of hits in the xy road is denoted by N_{xy}, and the standard PPHO requirement is denoted by "NoTrk". See text for details.

The first object listed in table 1, e_t, is referred to as a *tight* electron, and is required to have a CDC or FDC track pointing to the associated calorimeter cluster. The track does not necessarily point back to the primary vertex identified by RECO. The second object, e_l, is referred to as a *loose* electron. Since no tracking requirements are made, the cluster may or may not be associated with a track. If drift chamber hits are found (by HITSINFO) in the xy view between the cluster and the beamline, the object is referred to as a $\bar{\gamma}$. If no tracks are associated with the cluster, it is called a γ, and if no hits are found in the road, the object is called a *tight* photon (γ_t). Finally, if no tracks are found in a window of $\Delta\theta \times \Delta\phi = 0.2 \times 0.2$, the object is classified as a PPHO. The standard reconstruction algorithm only considers tracks in the 0.2×0.2 window defined by the calorimeter cluster and the primary vertex identified by RECO.

3. Trigger Bias

Since energy resolutions and corrections differ for hadronic and electromagnetic showers, it is necessary to impose kinematic requirements on the reconstructed objects to minimize trigger threshold bias on the ratios $P_{j\to\gamma}$ and $P_{j\to e}$. As shown schematically in figure 1, an event will tend to trigger more often near the trigger threshold E_T^0 when the leading object is isolated from hadronic activity and contained primarily in the electromagnetic calorimeter. Consequently, the e/γ populations are inflated relative to jets near the trigger threshold, and the ratios $P_{j\to e}$ and $P_{j\to\gamma}$ exhibit trigger-induced bumps.

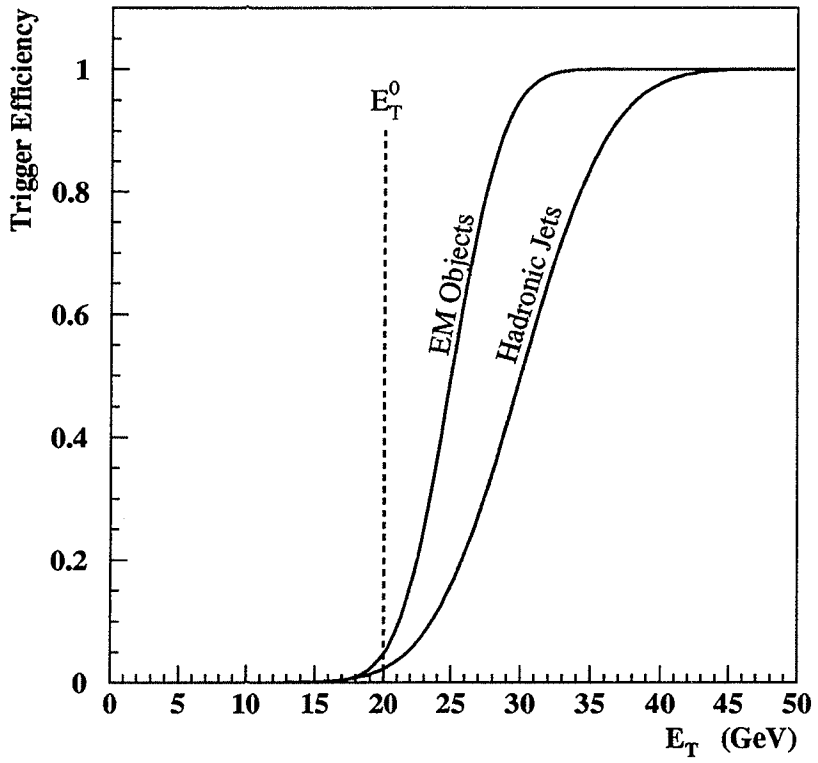

Figure 1: Typical trigger efficiencies for electromagnetic and hadronic objects as a function of transverse energy. The efficiency at the trigger threshold E_T^0 is not 50% due to offline energy corrections.

To avoid these biases, events are rejected if the leading object has transverse energy less than a threshold $E_T^{\rm Min}$ associated with the L2 filter which the event satisfied. This threshold is chosen such that the trigger is fully efficient for both electromagnetic and hadronic

showers. Table 2 summarizes the leading object transverse energy thresholds used in this measurement.

L2 filter	L1 E_T	L2 E_T	E_T^{Min}
jet_20	10	20	30
jet_30	15	30	50
jet_50	15	50	90
jet_85	35	85	150
jet_max	45	115	200

Table 2: Summary of E_T thresholds used in measuring fake rates. Units are GeV.

Figures 2 and 3 show the jet and $e + \gamma$ spectra, respectively, after all cuts in this section have been imposed. The relative population differences as a function of E_T are due kinematic requirements as well as relative trigger prescales.

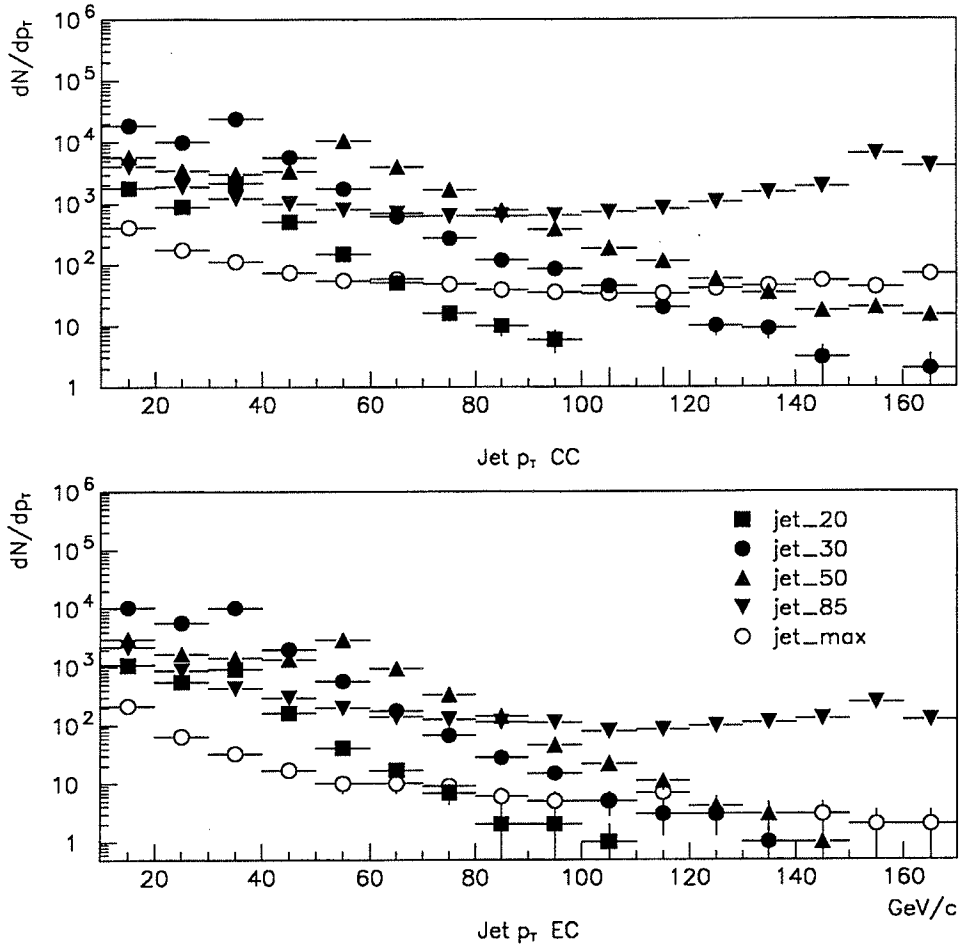

Figure 2: Transverse energy distribution of jets in the multijet sample for the central (CC) region and forward (EC) regions for the various filters used in this study.

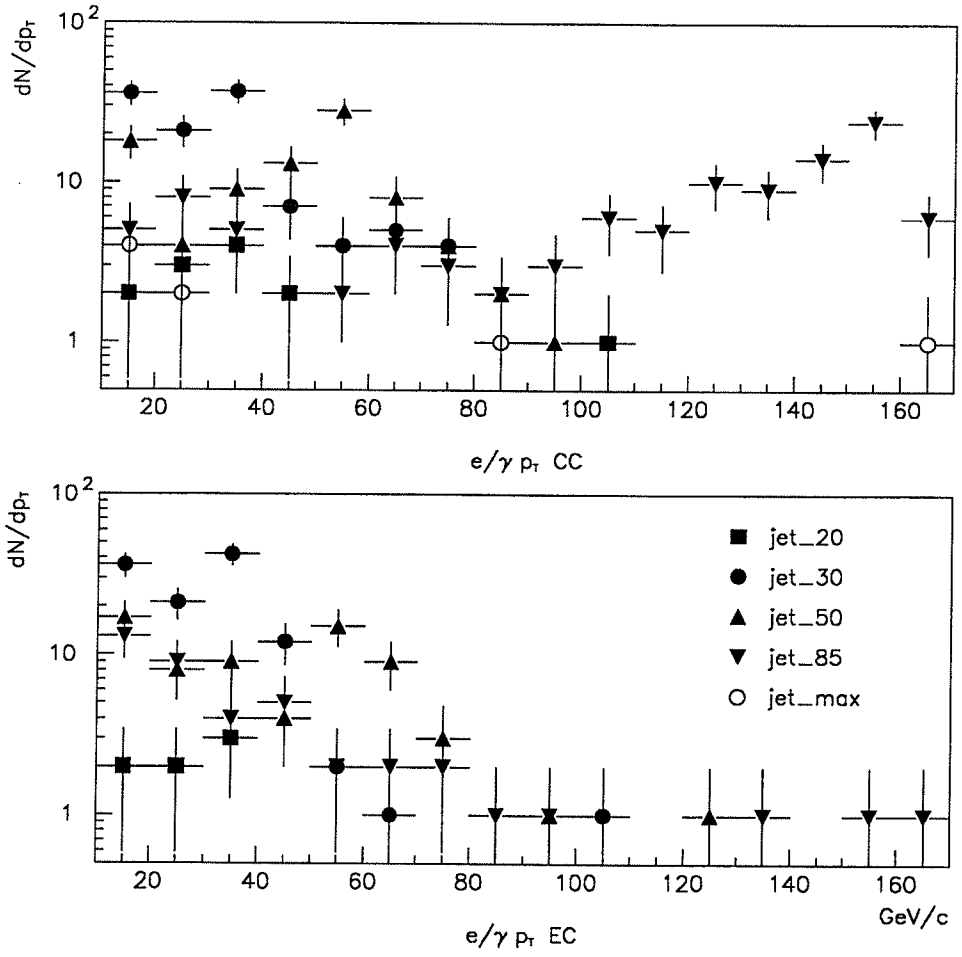

Figure 3: Transverse energy distribution of electrons and photons in the multijet sample for the central (CC) region and forward (EC) regions for the various filters used in this study.

3. Direct Photon Subtraction

Since multijet cross sections are much larger than W/Z cross sections, it is expected that the sample mentioned previously would be composed nearly entirely of QCD jets, and that any electrons or photons identified in the sample would arise from misidentified jets. However, the cross section for direct photon production is relatively large, and it increases relative to the multijet cross section at high p_T. (This is due in part to the fact that the electroweak coupling strength, α, increases as q^2 increases, while the strong coupling strength, α_s, decreases.) Therefore, it is important to subtract the direct photon component out of the sample before forming the ratio $P_{j\to\gamma}$.

In run 1A, it was determined [5] that the fraction of an inclusive isolated photon sample due to π^0 or η meson production could be parameterized by the function

$$f_{\gamma\gamma} = a \times e^{-b \times E_T}$$

where a and b are constants. The meson fraction was measured by comparing the longitudinal shower profile of photon candidates to predictions from the DØGEANT detector simulation. (Single photons are less likely to deposit energy in the first layer than two photons.) The results of the analysis were:

$$a = 1.14 \pm 0.05$$

and

$$b = 0.0177 \pm 0.0021 \text{ GeV}^{-1}$$

for photons in the CC subject to slightly different cuts than are employed here. The main difference is that the direct photon candidate selection requires the transverse energy in the isolation cone to be less than 2 GeV, while the isolation requirement in this study requires that the energy in the isolation cone be less than 10% of the energy in the core. (The two requirements are equivalent for a 20 GeV cluster at $\eta = 0$.) It is assumed here that the above measurement of the meson fraction is a close approximation to that which would be obtained if $W\gamma/Z\gamma$ analysis cuts were used. Since the latest DØ results [6] indicate that the meson fraction in the forward region is similar to the central region, it is assumed that the above measurement is approximately valid for EC photons as well. Finally, since the meson fraction measurement had a systematic uncertainty of 20% at $E_T = 20$ GeV [5], a systematic uncertainty of 30% is assigned to the meson fraction for this study to include any possible extrapolation errors to the selection criteria used in diboson analyses.

Jets can be misidentified as electrons if one or both of the photons from meson decay convert to an e^+e^- pair or if a soft charged hadron (from the jet or underlying event) overlaps the photon pair. As can be seen from figure 4, the number of electrons and photons in the multijet sample is approximately equal for $E_T > 30$ GeV. Since the conversion probability in

the central region is about 10% for (single) photons, it can be concluded that there are many more electrons than would be expected from γ or $\gamma\gamma$ conversions alone. Therefore, a substantial contribution to the fake electron rate must be due to charged hadron overlaps. This effect is reproduced by the ISAJET Monte Carlo [2]. Since the numbers of fake electrons and photons in the high E_T region are roughly equal, the direct photon contribution to fake electrons can be at most 10%, if all photons in the sample were due to direct photon production. This is a relatively small correction considering the size of the systematic uncertainty on the direct photon contribution itself. Therefore, no direct photon subtraction is performed on the fake electrons[‡]. In any case, a conservative systematic uncertainty of 30% is assigned to the fake electron probability to account for any possible electron contamination in the multijet sample.

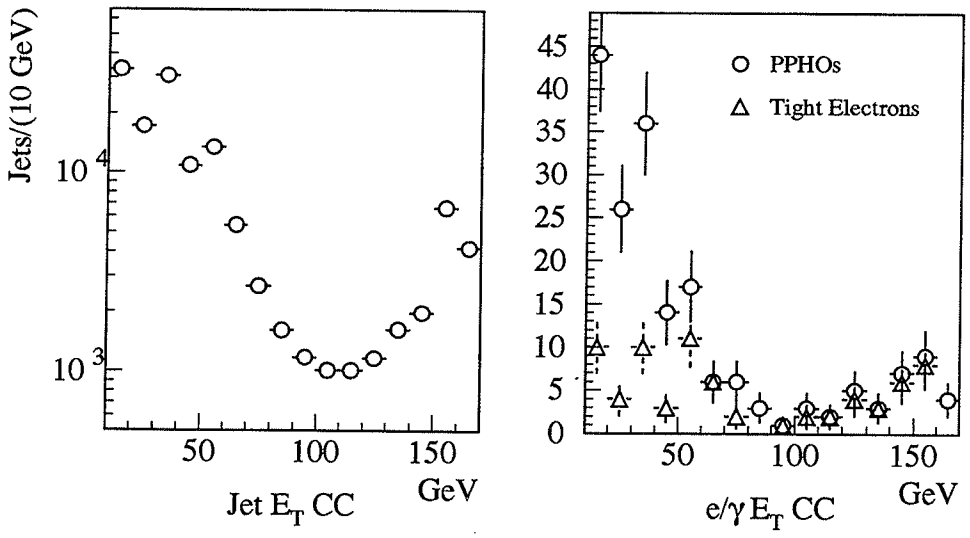

Figure 4: Jet, electron, and photon CC candidates identified in the multijet sample.

[‡]Since loose electrons (e_l) are not subject to tracking requirements, the candidates in the multijet sample have a contribution from direct photons, and the appropriate subtraction is performed in this case.

5. Fake Probabilities

After the corrections of the previous section have been applied to the photon populations, equations (1) and (2) are used to calculate the fake probabilities. Figures 5 and 6 show these rates as a function of transverse energy. The error bars displayed are Gaussian (symmetric) approximations to binomial uncertainties on the population ratios. It is evident that the probability for a jet to be misidentified as an electron increases at high E_T. A possible interpretation of this effect is that hadronization to single π^0/η becomes less likely as the jet E_T increases. Conversely, the fake photon probabilities decrease at high E_T, since the the isolated leading neutral mesons are more likely to be misidentified as electrons than at low E_T.

For each of the objects listed in table 1 and each corresponding plot in figures 5 and 6, the E_T-dependent fake probability is parameterized by the linear function

$$P = a_0 + a_1 E_T$$

where a_0 and a_1 are constants determined by a fit to the data and E_T is measured in units of GeV. Table 3 lists the fitted values of a_0 and a_1.

Object Type	CC		EC	
	$a_0 \times 10^3$	$a_1 \times 10^5$	$a_0 \times 10^3$	$a_1 \times 10^5$
e_t	-0.173 ± 0.20	1.43 ± 0.51	0.528 ± 0.86	5.09 ± 2.3
e_l	1.27 ± 0.34	0.300 ± 0.73	2.66 ± 0.11	3.13 ± 2.7
$\bar{\gamma}$	0.0754 ± 0.29	2.06 ± 0.70	1.32 ± 1.0	6.31 ± 0.27
γ	1.45 ± 0.19	-1.06 ± 0.41	2.01 ± 0.38	-2.1 ± 1.0
γ_t	1.08 ± 0.17	-0.845 ± 0.352	0.64 ± 0.11	-
PPHO	1.19 ± 0.16	-1.03 ± 0.33	0.97 ± 0.14	-

Table 3: Jet misidentification probabilities for electrons and photons. Errors quoted are statistical (fit) errors only. A systematic uncertainty of 30% is assigned to each fake probability. See table 1 for definitions of object types. Uncertainties are statistical only.

The following conclusions can be drawn regarding the jet misidentification probabilities:

- The requirement of a track or hits reduces the fake rate by about a factor of 5 for central electrons. The track requirement results in about 1/3 fewer fake central electrons relative to electrons subject only to drift chamber hit requirements.

- The fake rates for central photons are improved slightly (5-10%) if a drift chamber hit veto is imposed.

- Due to the high track density in the forward region, the electron fake rate is 5-10 times higher in the EC than in the CC. The photon fake rate for the EC is similar to that for the CC.

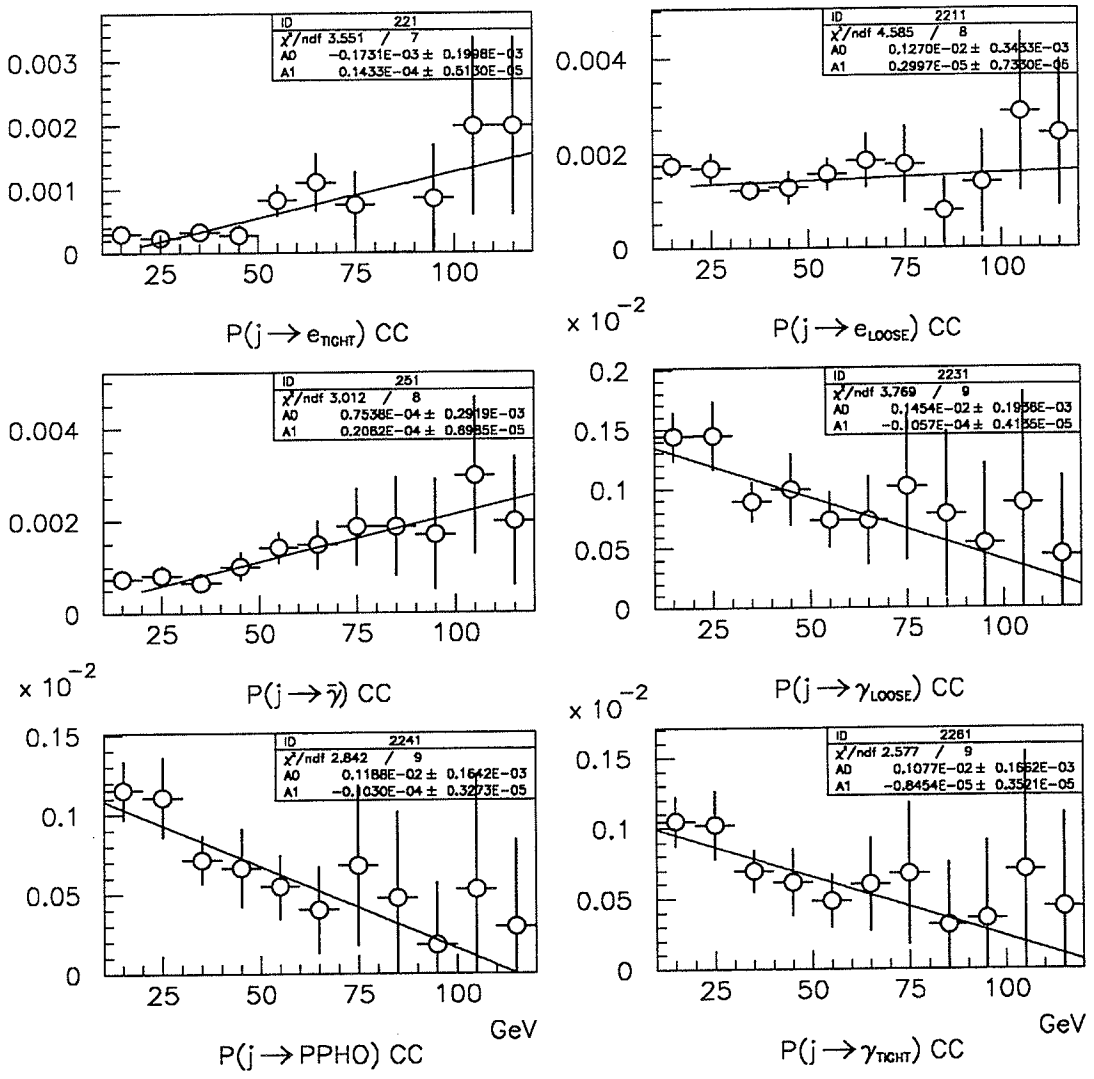

Figure 5: Jet misidentification probabilities for jets in the CC.

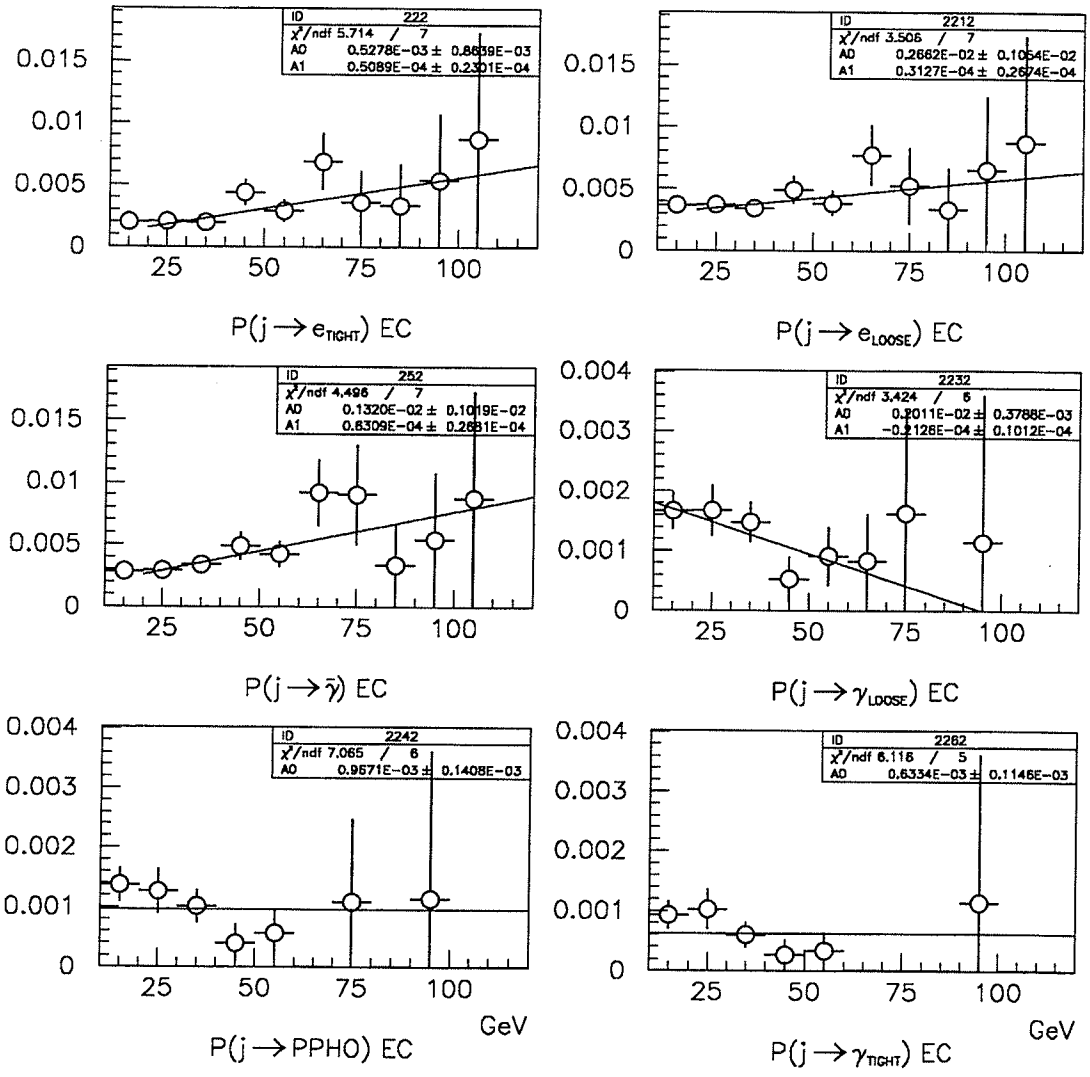

Figure 6: Jet misidentification probabilities for jets in the EC.

6. Verification: background prediction for $Z \rightarrow ee$

To investigate the validity of the above procedures, the fake electron probabilities in table 3 can be applied to a multijet sample and compared to dielectron data. Specifically, the predicted fake ee spectrum from the `jet_20` data should match the background observed in $Z \rightarrow ee$ candidates collected from the `em2_eis2_hi` filter.

To make the comparison as legitimate as possible, the kinematic requirements on jets are the same as those imposed on electrons:

- $E_T > 25$ GeV
- $|\eta_{\text{Cal.}}| < 1.0$ or $1.5 < |\eta_{\text{Cal.}}| < 2.5$

It should also be noted that although `jet_20` and `em2_eis2_hi` require objects with $E_T > 20$ GeV, `em2_eis2_hi` is slightly more efficient near threshold for electrons relative to `jet_20` for jets due to the difference in electron and jet energy resolutions. Figure 7 shows the jet E_T spectrum and the jet distribution after selection criteria have been applied. The apparent depletion of jets near $E_T = 25$ GeV is due to trigger resolution.

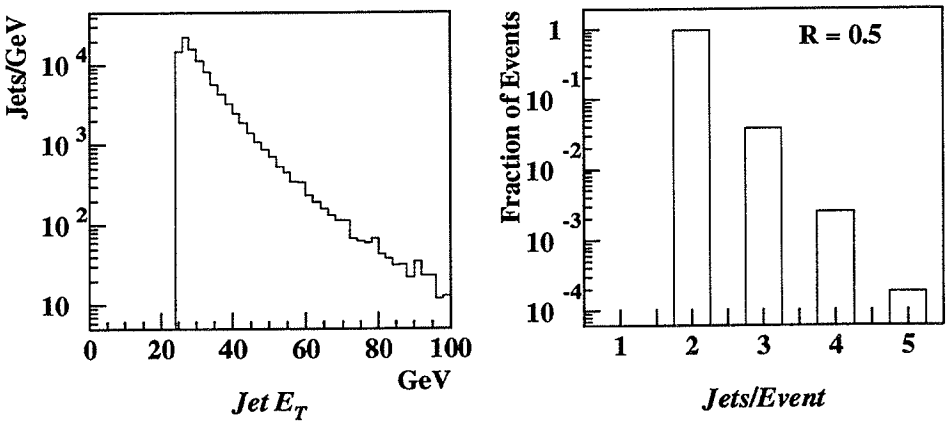

Figure 7: Left: transverse energy distribution of jets in multijet candidate events. Right: distribution of the number of jets per event. See text for selection criteria.

The probability for a dijet pair to be misidentified as a dielectron pair is given by

$$P_{jj \rightarrow ee} = P_1 P_2$$

where P_1 and P_2 are the individual fake probabilities for each of the two jets. In events with more than two jets, the number of possible dijet combinations, N_{jj}, is given by

$$N_{jj} = \frac{N_j!}{2!(N_j - 2)!}$$

where N_j is the number of jets in the event satisfying the desired kinematic requirements. Assuming only one dijet pair per event can result in a dielectron fake at a time, the probability for a *given pair* to result in a dielectron fake is P_{jj} multiplied by the probability that no other pairs in the event result in a fake pair. In other words, the probability that jets i and j fake the ee signal is given by

$$P_{ij} = P_i P_j \prod_{n,m \neq i,j} (1 - P_n P_m) \tag{3}$$

and the probability that *any one pair* fluctuates is given by

$$P = \sum_{i,j} P_i P_j \prod_{n,m \neq i,j} (1 - P_n P_m).$$

In practice, the correction in equation (3) is small, as less than 5% of the multijet events contain more than two jets which satisfy the kinematic requirements outlined previously. See figure 7 for details.

The final factor to consider is the relative luminosities of the dielectron and multijet samples. The dielectron sample[§] corresponds to 72 pb^{-1}, and the multijet sample corresponds to 6.0^{-1} nb, so the predicted number of fake dielectrons must be multiplied by 1.20×10^4 before comparing them to those in the dielectron candidate sample.

Using the fake probabilities for e_t and $\bar{\gamma}$ from table 3, the dielectron fake probability from equation 3, and summing over all possible dijet combinations per event, the fake dielectron spectrum shown in figure 8 is obtained. The predicted background is approximately linear in shape and matches the observed dielectron mass spectrum quite well. In the sidebands on either side of the $Z \rightarrow ee$ peak, the predicted background spectrum is lower than the observed ee spectrum, but the ee spectrum is expected to contain Drell-Yan pairs in addition to fakes. However, the predicted background matches the ee sidebands within the $\sqrt{2} \times 30\%$ systematic uncertainty assigned to the dielectron fake rate, and the agreement improves in the 130-150 GeV bin.

[§]Since drift chamber hit information is available only from μDST's reconstructed with RECO 12.15 and higher, data which was reconstructed with previous versions were not used.

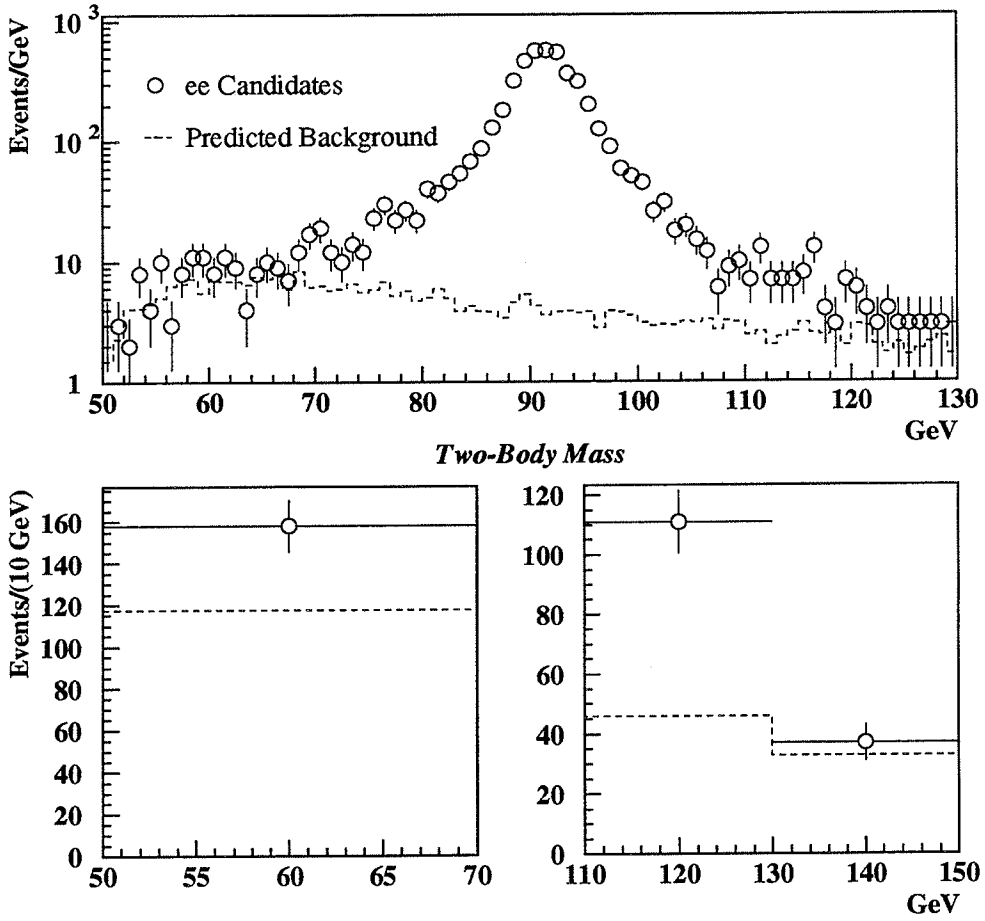

Figure 8: Top: Invariant mass of dielectron candidates and predicted multijet background. Bottom: Invariant mass spectrum of dielectron candidates and predicted multijet background for the sidebands on either side of the $Z \rightarrow ee$ peak. Systematic and statistical error bars on the background prediction have been omitted for clarity.

Conclusions

A measurement of the probabilities at which jets are misidentified as electrons or photons in 1B data has been presented. Effects due to trigger bias and direct photons have been accounted for. Generally, the fake rates are about 10^{-3}, and the rate for electrons rises as the jet transverse energy increases. Photon fake rates decrease slightly as the jet transverse energy increases. Application of the fake probability to a multijet sample reproduces the background to $Z \rightarrow ee$.

Acknowledgments

This work has benefited greatly from the insights of the previous studies given in the reference section. The author is indebted to T. Fahland for cross checking the results.

References

1. D. Chakrobarty and M. Fatyga, "QCD Backgrounds to Electroweak Signals: A Study of Electron and Fake Photon Probability". DØ Note 1753.

2. M. Fatyga, "A Comparison of Fake Electron Rates in Data and the ISAJET Monte Carlo. A Comparison of Multi-Jet Triggers with ISAJET Monte Carlo". DØ Note 1850.

3. M. Kelly, "Jet Faking Photon/Electron Study". DØ Note 1659.

4. M. Kelly, "The Doomsday Study of QCD Flakes for $W\gamma$ in RECO 11". DØ Note 2215.

5. S. Fahey, "Direct Photon Production at $\sqrt{s} = 1.8$ TeV". PhD. thesis (unpublished), 1995.

6. S. Abachi *et al.*, "The Isolated Photon Cross Section in the Central and Forward Rapidity Regions in $p\bar{p}$ Collisions at $\sqrt{s} = 1.8$ TeV", FERMILAB-PUB-96-072-E, 1996.